Letter

Quantum simulation of indefinite causal order induced quantum refrigeration

Huan Cao,[*] Ning-Ning Wang,[*] Zhian Jia, Chao Zhang,[†] Yu Guo, Bi-Heng Liu, Yun-Feng Huang,[‡] Chuan-Feng Li,[§] and Guang-Can Guo

CAS Key Laboratory of Quantum Information, University of Science and Technology of China, Hefei 230026, China and CAS Center For Excellence in Quantum Information and Quantum Physics, Hefei 230026, China

(Received 26 January 2021; revised 9 August 2021; accepted 10 June 2022; published 16 August 2022)

In the classical world, physical events always happen in a fixed causal order. However, it was recently revealed that quantum mechanics allows events to occur with indefinite causal order (ICO). In this study, we use an optical quantum switch to experimentally investigate the application of ICO in thermodynamic tasks. Specifically, we simulate the working system interacting with two identical thermal reservoirs in an ICO, observing the quantum heat extraction even though they are in thermal equilibrium where heat extraction is inaccessible by traditional thermal contact. Using such a process, we simulate an ICO refrigeration cycle and investigate its properties. We also show that by passing through the ICO channel multiple times, one can extract more heat per cycle and thus obtain a higher refrigeration performance. Our results suggest that the causal nonseparability can be a powerful resource for quantum thermodynamic tasks.

DOI: 10.1103/PhysRevResearch.4.L032029

Introduction. It is a deeply rooted concept that in a physical theory, there is a well-defined pre-existing classical causal structure for which physical events happen. However, from the Bell-Kochen-Specker theorem [1,2], quantum mechanics is incompatible with the viewpoint that observables have pre-existing values independent of the measurement. Inspired by this, recent studies have shown that if we assume the causal relation to obey the laws of quantum mechanics, it is possible for two events to occur with superposed causal orders. Thus, there is no pre-existing causal relation [3,4]. The quantum causal structure becomes especially crucial when quantum physics and general relativity become relevant [5–9]. A typical example is the quantum spacetime causal structure in the study of quantum gravity [10–14].

Besides the fundamental properties of indefinite causal order (ICO), the applications of ICO as an operational resource in quantum protocols also attract considerable interests [15,16]. It provides remarkable enhancements ranging from channel discrimination [17], communication and computation complexity [18–20] to quantum metrology [21,22], quantum information transmission [23–25] etc. Recently, some of them have been experimentally studied by simulating ICO process with optical quantum switch [26–31].

In thermodynamics, entropy in closed systems always tends to increase definitely. An interesting question is what about applying ICO in thermodynamic tasks. One such example is the recent discovery of ICO-based quantum refrigeration [32]. There are several different ways for refrigeration: the standard one is powered by energy injected by a time-dependent driving force [33,34]; the Maxwell demon can steer the heat with feedback control loops [35,36]; while another method is using invasive quantum measurements as a resource [37]. All the above refrigeration protocols work in pre-existing causal structures. The ICO-based protocol provides a good supplement where no preexisting causal relation is assumed [22,32,38–41].

In this Letter, by faithfully adopting the protocol and extending the strategy in Ref. [32], we experimentally simulate the ICO induced heat extraction by optical quantum switch and investigate its feasibility to construct a quantum refrigerator, while in the mean time an independent similar experiment was made by Nie *et al.* with an equivalent circuit on nuclear spins using the nuclear magnetic resonance system [42]. We also show that by interacting with reservoirs in ICO multiple times, one can extract more heat from the reservoirs per cycle. The high accuracy achieved in our experiment will motivate more operational protocols and contribute to broader research into ICO.

Protocol outline. Consider a system with Hamiltonian $\mathcal{H}$ and energy eigenstates $|n\rangle$ for energy level E_n. After thermocontact with a thermal reservoir with inverse temperature β, the resulting equilibrium state of the system is always $T = e^{-\beta\mathcal{H}}/Z = \sum_n e^{-\beta E_n}/Z|n\rangle\langle n|$ regardless of the initial system state ρ, where $Z = \mathrm{Tr}(e^{-\beta\mathcal{H}}) = \sum_n e^{-\beta E_n}$ is the partition function. This thermodynamics operation can be characterized by a completely positive trace preserving (CPTP) map $\mathcal{T} : \mathcal{L}(\mathcal{H}) \to \mathcal{L}(\mathcal{H})$ for which $\mathcal{T}(\rho) = T$ for all density operators ρ. The Kraus decomposition is $\mathcal{T}(\rho) = \sum_i K_i \rho K_i^\dagger$, where the Kraus operators $\{K_i\}$ satisfy $\sum_i K_i^\dagger K_i = I$.

Consider the situation where the system state ρ undergoes thermocontact sequentially with two identical thermal

[*]These two authors contributed equally to this work.
[†]drzhang.chao@ustc.edu.cn
[‡]hyf@ustc.edu.cn
[§]cfli@ustc.edu.cn

reservoirs. If we assume the definite causal order, then the process is given either by $\mathcal{T}^1 \circ \mathcal{T}^2(\rho)$ or $\mathcal{T}^2 \circ \mathcal{T}^1(\rho)$, or potentially a classical probabilistic mixture of them. The thermal state T is always obtained. However, when applying ICO, the two events "thermocontact with thermal reservoir 1 firstly" and "thermocontact with thermal reservoir 2 firstly" can occur in a superposed causal order. An intriguing phenomenon arises—the resulting state is different from T. Such an operation can be simulated using the quantum switch [17,26,43]. The action of ICO is achieved by routing particles through two channels with the visiting order being tailored by the control qubit [26–31]. When the control qubit is $|\phi_c\rangle = |1\rangle$ ($|0\rangle$), the operations $\mathcal{T}^2 \circ \mathcal{T}^1 (\mathcal{T}^1 \circ \mathcal{T}^2)$ are carried out respectively. We denote the corresponding channel as $\mathcal{S}^T$. In terms of Kraus operators, we have $\mathcal{S}^T(\rho_c \otimes \rho) = \sum_{ij} M_{ij}(\rho_c \otimes \rho)M_{ij}^\dagger$ and

$$M_{ij} = |0\rangle\langle 0|_c K_i^1 K_j^2 + |1\rangle\langle 1|_c K_j^2 K_i^1, \tag{1}$$

where K_i^1 (K_j^2) represents the ith (jth) Kraus operator of the thermalizing channels $\mathcal{T}^1$ ($\mathcal{T}^2$).

Considering simplest nontrivial case, a two-level system, the ground (excited) state is $|0\rangle$ ($|1\rangle$) with energy $E_0 = 0$ ($E_1 = \Omega$), thus, the Hamiltonian for the system is $\mathcal{H} = \Omega|1\rangle\langle 1|$. The thermal state at a given temperature is $\rho = \mathrm{diag}(1, e^{-\beta\Omega})/Z$, where $Z = 1 + e^{-\beta\Omega}$. In the following we set $\Omega = 1$ for simplicity. If the ancillary control qubit is initialized as $|\phi_c\rangle = (|0\rangle + |1\rangle)_c/\sqrt{2}$, the output state undergoing ICO with two identical thermalizing channels is

$$\begin{aligned}\mathcal{S}^T(\rho_c \otimes \rho) = \tfrac{1}{2}[&(|0\rangle\langle 0|_c + |1\rangle\langle 1|_c) \otimes T \\ &+ (|0\rangle\langle 1|_c + |1\rangle\langle 0|_c) \otimes T\rho T],\end{aligned} \tag{2}$$

where the control qubit is $\rho_c = |\phi_c\rangle\langle\phi_c|$. Note that the control qubit gets entangled with the system during ICO evolution; if the control qubit is projected into $|\pm\rangle = (|0\rangle \pm |1\rangle)_c/\sqrt{2}$, the system collapses into

$$\mathrm{Tr}_c[|\pm\rangle\langle\pm|_c \mathcal{S}^T(\rho_c \otimes \rho)] = \tfrac{1}{2}(T \pm T\rho T), \tag{3}$$

with probability $p_\pm = \frac{1}{2}\mathrm{Tr}[T \pm T\rho T]$. Noting that the temperature of output system state could be different from the thermal state T. This intriguing phenomenon suggests that the ICO can either extract heat from or dump heat into the reservoir.

Experimental implementation. We simulate the ICO process with tabletop photonic quantum switch. Twin photons at 780 nm are generated by spontaneous parametric down conversion and one of them is detected as the trigger. The other one named heralded photon acts as the working substance and is then fed into a Mach-Zehnder interferometer (Fig. 1). We utilize photonic polarizations to mimic the two energy levels of the working system where horizontal (vertical) polarization state H (V) represents the ground (excited) state [44,45]. In that way, the population of excited state represents the energy of the working system $\mathrm{Tr}(\rho\mathcal{H}) = e^{-\beta\Omega}/Z$ and hence reflects the temperature of the working system. A system state at an arbitrary temperature is prepared by randomly rotating the photonic polarization into H or V with a probability proportional to its temperature. Energy detection can be realized by measurements in Pauli σ_z basis; thus, the temperature can be inferred. A beam splitter (BS1) introduces two spatial modes

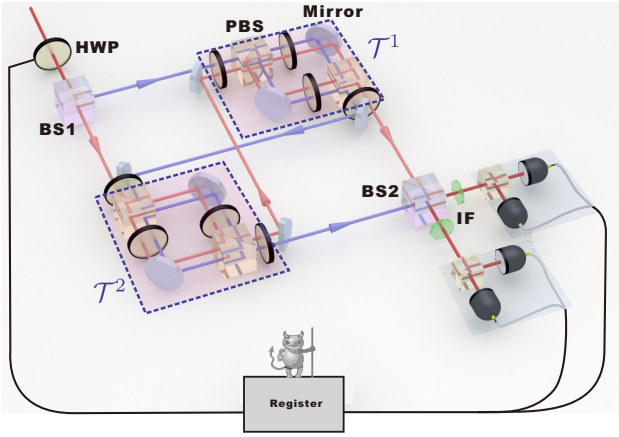

FIG. 1. Experimental apparatus. The quantum switch contains two identical thermalizing channels (with pink planes underneath) in an indefinite causal order. One of the causal orders is presented by a bluish optical path, the other is presented by a red one. BS: beam splitter; PBS: polarization beam spliter; HWP: half wave plate; IF: interference filter.

as the control qubit. The polarization qubit undergoes the causal order $\mathcal{T}^1 \circ \mathcal{T}^2$ in one spatial mode, while $\mathcal{T}^2 \circ \mathcal{T}^1$ in the other. BS2 then coherently combines spatial modes and projects the control qubit onto $|\pm\rangle$. It is reasonable to accept that the switch channel is accomplished when the two spatial modes form an interferometer [26,29,31], while more rigorous verification of the ICO process requires measuring the witness [27]. A phase-locking system is adopted to ensure the stability of the path interferometer with an average interferometric visibility of more than 99.7% [46]. The interaction of system qubit with reservoirs can be modeled by two processes with the happening rate dictated by the temperature: (i) The qubit releases the energy to reservoir and decays to ground state; (ii) The qubit absorbs an excitation from reservoir and hops into the excited state. The generalized amplitude damping channel (GAD) explicitly simulates this interaction [45,47,48]. The GAD is decomposed into $\mathcal{T}(\rho) = \sum_{i=1}^4 K_i \rho K_i^\dagger$, of which the $\{K_1, K_2\}$ ($\{K_3, K_4\}$) forms a standard amplitude damping channel describing the process (i) (ii). For realization of the sequential thermalizing channel, 16 Kraus operator settings $\{K_i \otimes K_j, i, j = 1, 2, 3, 4\}$ are randomly implemented and mixed classically, while two branches of interferometer is coherently combined without destroying the superposition We performed the process tomography of the thermalizing channel at different temperatures. The average process fidelity exceeds 99.9%, verifying the credible simulation of the channel [46].

Results of ICO induced heat extraction. We first verify the nonclassical heat extraction driven by the ICO. We implement experiments by traversing the temperatures of the thermalizing channel. The system is initialized into the thermal state with the same temperature ($1/\beta_C$) as reservoir $\rho = T$. Fig. 2(a) shows the measured energy change ΔE of the system qubit (as working substance) after passing through the ICO channel. In the xcoordinate, we use energy of the thermal state to represent the reservoir's temperature for simplicity. By extrapolating experimental data [red and blue dots in Fig. 2(a)]

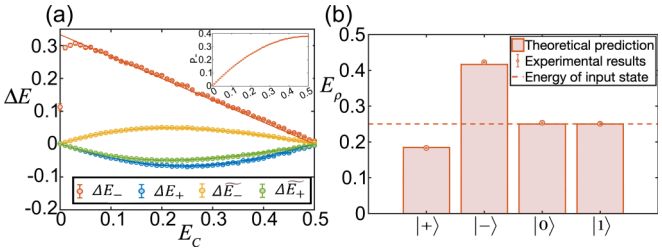

FIG. 2. (a) Energy change $\Delta E_\pm = \mathrm{Tr}(\rho_\pm \mathcal{H}) - \mathrm{Tr}(\rho \mathcal{H})$ where $\rho_\pm = [T \pm T\rho T]/\mathrm{Tr}[T \pm T\rho T]$ is the normalized output system state with the control qubit measured in $|\pm\rangle$. The weighted energy change is presented as $\Delta \widetilde{E}_\pm$. The horizontal coordinate $E_C = e^{-\beta_C}/(1 + e^{-\beta_C})$ ranges from 0 to 0.5. (b) Energy of the working system $E_\rho = \mathrm{Tr}(\rho \mathcal{H})$ when the control qubit is measured at $|+\rangle, |-\rangle, |0\rangle, |1\rangle$. The quoted error reflects the impact of Poissonian statistics on the collecting count.

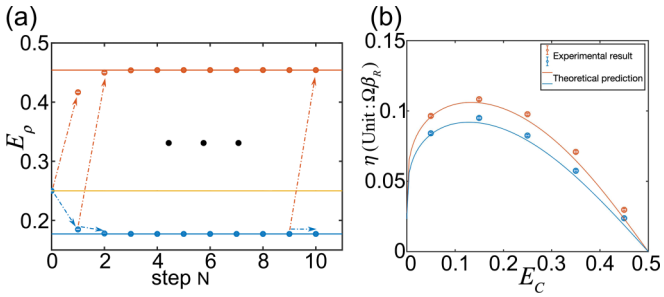

FIG. 3. (a) Energy of the working system after passing through the ICO channel multiple times. Each step will generate a two-component outcome. The latter step is performed only when the former step yields a failed outcome $|+\rangle$ (multi-pass condition, as shown by the arrows in each step, with intermediate ones abbreviated with ellipsis). The saturated energy in both outcomes is indicated by red and blue lines. (b) Coefficients of performance based on the classical strategy (blue) and multipass strategy (red). Here the coefficient is calculated in steady-state solution.

to theoretical prediction [red and blue lines in Fig. 2(a)], we find that the working substance can extract the heat flow from the reservoir when the control qubit is measured in $|-\rangle$ (initially prepared into $|+\rangle$), even though they initially share the same temperature. This intriguing phenomenon is applicable in arbitrary temperature cases except for zero and infinity. The heat extraction decreases when the temperature increases, whereas the successful probability $p_- = \mathrm{Tr}[|-\rangle\langle -|\mathcal{S}^T(\rho_c \otimes \rho)]$ increases [inset in Fig. 2(a)]. The weighted energy change $\Delta \widetilde{E}_\pm = p_\pm \Delta E_\pm$ is also presented [orange and green dots and lines 2(a)]. In the absence of information of control qubit's status by tracing it out, the averaging energy change strictly sums up to a vanishing value $\Sigma_{k=\pm} \Delta \widetilde{E}_k = 0$ both for experimental and theoretical data. This indicates that the heat extraction between thermal equilibrium systems can never occur spontaneously, in accord with Clausius statement of the second law of thermodynamics [49].

For comparison, energy transfer with control qubit measured in a computational basis $\{|0\rangle, |1\rangle\}$ is also performed, by exemplifying the reservoir's temperature $E_C = 0.25$ [Fig. 2(b)]. Such a case stands for the fixed causal order or equivalently the working substance classically contacting with reservoirs where they share a single temperature. This yields a trivial result that no heat extraction could achieve because classical thermocontact can not extract any heat flow from reservoirs at a single temperature; however the limitation can be broken by introducing ICO between reservoirs.

Obviously, the quantum heat extraction driven by ICO can be used for thermodynamic tasks. For example, when working substance appears at the heating component, we can make it interact with an external hot reservoir to release heat, thus refrigerating the reservoir; otherwise, we may send it back to the reservoir to erase the unwanted heat exchange. An interesting question is whether the working substance can become colder or hotter after passing through the ICO channel multiple times.

Our second result investigates this multipass strategy. We start with the working substance at the same temperature as the reservoirs. As an example, we still adopt the initial temperature to the one such that $E_C = 0.25$. At each step, a single run of quantum switch is carried out. Hence one initial state will generate a two-component outcome [indicated by the arrows in Fig. 3(a)]. Here we only consider the case in which the working substance becomes colder and then send it into the next step as initial state. In the experiment, photons will be annihilated after being measured in each step, so we use the measurement results (classical information) to determine the state preparation in the next step to simulate this iterative process (as the loop depicted in Fig. 1). The experimental results for the 10-step ICO are summarized in Fig. 3(a), in which the iteration process is indicated by the arrows. We observe that when the multipass ($N \geqslant 2$) ICO is implemented, a colder working substance in the unwanted component could jump into a higher temperature compared to in the single-step process ($N = 1$). This means that the multi-pass ICO may release the restriction for the external reservoir for heat dumping. Interestingly, Fig. 3(a) shows that the working substance will quickly saturate to a specific temperature, which means the output working substance remains unchanged in its input state when the control qubit is measured to be $|+\rangle$. We theoretically calculate this steady-state solution for all temperatures of the reservoir and also experimentally sample five points $E_C = \{0.05, 0.15, 0.25, 0.35, 0.45\}$, finding that the working substance always tends toward this steady-state solution after several iterations [46].

Construction of a quantum refrigerator. Considering the refrigeration task driven by ICO, an operational cycle is constructed with the diagram of a single cycle shown in Fig. 4. Stroke (i), Initialize the working substance by classically interacting with the cold reservoir (preparing a colder working substance required additional work cost, thus is excluded in our discussion). Then interacts with the two cold reservoirs superposed in ICO. Stroke (ii), Measure the control qubit. If the control qubit is collapsed into $|-\rangle$, the working system successfully extracts heat from the cold reservoir, followed by proceeding to the next stroke. Otherwise, two alternative strategies are available: (a) the working system classically contacts the cold reservoir to recover its initialized state, thereby undoing the unwanted heat change, and a new cycle is implemented (termed classical strategy); (b) the ICO is repeatedly passed through until the desired outcome is

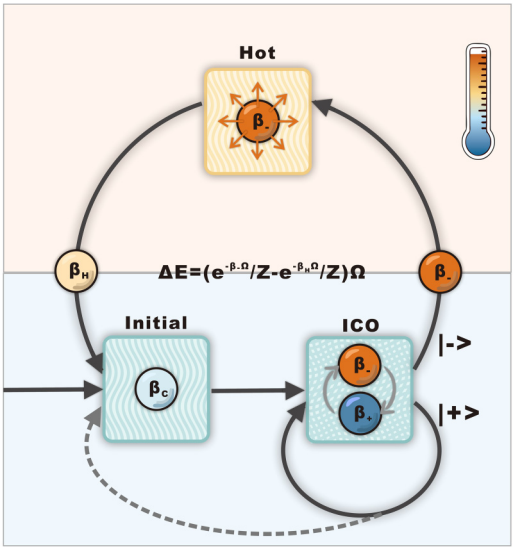

FIG. 4. Diagram of single cycle of quantum refrigerator. The reservoirs are denoted by squares and the working substance is denoted by the ball with the color corresponding to its temperature. Two recycling strategies are presented by the dotted arrow (classical strategy) and solid arrow (multi-pass strategy). The icon is taken from Ref. [41].

obtained (termed multi-pass strategy). Stroke (iii), the working substance makes classical thermocontact with the external hot reservoir for heat release; subsequently, a new cycle is started.

To evaluate the performance of the quantum refrigerator, we introduce the coefficient of performance, calculated by dividing the heat change from the cold reservoir by the work cost of measurement [50]. The total heat extraction per cycle ΔE is related to the temperature of particle entering (β_-) and leaving the external hot reservoir (β_H) (depicted by the particles on the centerline). Basically, the hot reservoir should not be hotter than the output working substance to release the heat so that it bounds the refrigerant range. Here, we fix $\beta_H = \beta_C$ to maximize the heat extraction, which yields $\Delta E = E_- - E_C$.

The magic of the ICO refrigerator can be explained by Maxwell's demon-like cooling mechanism. In each cycle of the quantum refrigerator, the control qubit is measured with results stored in register. The following operation is determined by the information of register. However, the ICO scheme only relies on projection of control qubit on fixed basis and thermalizing channels alone, which releases the requirement of microscopic measurements and manipulation on working systems [46]. Since we assume the control qubit has energy degeneracy, the measurement itself does not cost energy. Rather, the energy cost comes from resetting the register for proceeding to the next cycle, which refers to Landauer's erasure [51]. The work cost is $\Delta W = \frac{1}{\beta_R} S$, where $S = (p_+ \ln p_+ + p_- \ln p_-)$ is the Shannon entropy of the register and β_R is the inverse temperature of the resetting reservoir. Therefore the coefficient of performance is

$$\eta = -\frac{\Delta E}{\bar{n}\Delta W}, \tag{4}$$

where $\bar{n} = \frac{1}{p_-}$ is the average number of measurements consumed per cycle.

For a classical strategy, the coefficient of quantum refrigeration can be directly calculated by Eq. (4). For multipass strategy, it potentially contains many steps per cycle. The heat flow and work cost in each step is not identical. However, we can approximate the coefficient by assuming that the quantum refrigerator is working at the steady-state point because a single cycle is much more likely to undergo multiple steps and quickly evolve into equilibrium. (It will lead to slight overestimation. For more rigorous comparison, realistic averaged coefficient is also provided in [46]). We comparatively present the coefficients under both strategies in Fig. 3(b), where the solid lines (dots) show the theoretical prediction (experimental results) for sample temperatures $E_C = \{0.05, 0.15, 0.25, 0.35, 0.45\}$. The underlying idea of two strategies is how to cancel the heat exchange in unwanted direction, either by classical thermocontact to return or directly sending it into the next ICO step. The results show that the multi-pass strategy surpasses classical strategy, revealing the possibility of improving the efficiency of quantum thermodynamic tasks by introducing a more complex causal structure of the thermalizing channels.

Conclusions. Our work provides a paradigm of quantum machine alternative to ones driven by other nonclassical features [52,53]. Despite a measurement of inside strokes, both the outcomes are taken into account, hence the refrigerator does not depend on post-selection to gain advantages. In addition, we provided a possible setup by adopting an equivalent circuit without projective measurement where the feedback is controlled by control qubit [32,46]. This advantage of the ICO-driven protocol becomes crucial when the control qubit cannot be used for direct thermalization and the ICO process allows us to access the free energy of control qubit.

The second law of thermodynamics imposes the irreversibility on thermodynamical evolution where, as the system advances through time, the heat can only naturally flow from hot to cold but not vice versa. Our experiment clearly shows that superposition of thermal operation in ICO can project the process onto diffrent directions of heat flow, which is interesting for thermodynamics since previously the thermodynamics is established in predefined causal order. Notice that the initial system state is Gibbs state and the thermalizing channel is a thermal operation of a specific Hamiltonian [54]. Both of them are resource free in thermodynamical resource theory. It shows interests to thermodynamical resource theory that development of thermodynamical resource by allowance of thermal operation superposed in ICO (as well as measure of a control qubit) resulting in resourceful operation should be taken in to account. We expect that our work will advance further investigations on the exotic property of ICO, as well as its superiority in quantum thermodynamical tasks. Additionally, implementation of ICO based on high-performance optical quantum switch may encourage avenues on experimental research of other demanding ICO experiments like semi-device-independent certification of ICO [55], as well as measuring out-of-time-order correlation by adopting two superposed reversal sequential control order [56,57].

Acknowledgments. We thank Yong-Xiang Zheng, Xue Li, Xiao Liu for beneficial discussions. This work was supported by National Natural Science Foundation of China (11734015, 62075208, 11874345, 11821404), Science and Technological Fund of Anhui Province for Outstanding Youth (2008085J02).

[1] J. S. Bell, On the Einstein Podolsky Rosen paradox, Phys. Phys. Fiz. **1**, 195 (1964).
[2] S. Kochen and E. P. Specker, The problem of hidden variables in quantum mechanics, in *The Logico-Algebraic Approach to Quantum Mechanics* (Springer, Berlin, 1975), pp. 293–328.
[3] O. Oreshkov, F. Costa, and Č. Brukner, Quantum correlations with no causal order, Nat. Commun. **3**, 1092 (2012).
[4] Č. Brukner, Quantum causality, Nat. Phys. **10**, 259 (2014).
[5] D. Oriti, *Approaches to Quantum Gravity: Toward a New Understanding of Space, Time and Matter* (Cambridge University Press, Cambridge, 2009), pp. 1–150.
[6] S. Hossenfelder, *Experimental Search for Quantum Gravity* (Springer, Berlin, 2017).
[7] C. Marletto and V. Vedral, Gravitationally Induced Entanglement between Two Massive Particles is Sufficient Evidence of Quantum Effects in Gravity, Phys. Rev. Lett. **119**, 240402 (2017).
[8] S. Bose, A. Mazumdar, G. W. Morley, H. Ulbricht, M. Toroš, M. Paternostro, A. A. Geraci, P. F. Barker, M. S. Kim, and G. Milburn, Spin Entanglement Witness for Quantum Gravity, Phys. Rev. Lett. **119**, 240401 (2017).
[9] A. Peres and D. R. Terno, Quantum information and relativity theory, Rev. Mod. Phys. **76**, 93 (2004).
[10] M. Christodoulou and C. Rovelli, On the possibility of laboratory evidence for quantum superposition of geometries, Phys. Lett. B **792**, 64 (2019).
[11] B. S. DeWitt, Quantum theory of gravity. I. The canonical theory, Phys. Rev. **160**, 1113 (1967).
[12] C. Rovelli, Quantum mechanics without time: A model, Phys. Rev. D **42**, 2638 (1990).
[13] R. Gambini, R. A. Porto, and J. Pullin, A relational solution to the problem of time in quantum mechanics and quantum gravity: A fundamental mechanism for quantum decoherence, New J. Phys. **6**, 45 (2004).
[14] L. Hardy, Quantum gravity computers: On the theory of computation with indefinite causal structure, in *Quantum Reality, Relativistic Causality, and Closing the Epistemic Circle* (Springer, Berlin, 2009), pp. 379–401.
[15] M. M. Taddei, R. V. Nery, and L. Aolita, Quantum superpositions of causal orders as an operational resource, Phys. Rev. Research **1**, 033174 (2019).
[16] D. Jia and F. Costa, Causal order as a resource for quantum communication, Phys. Rev. A **100**, 052319 (2019).
[17] G. Chiribella, Perfect discrimination of no-signalling channels via quantum superposition of causal structures, Phys. Rev. A **86**, 040301(R) (2012).
[18] P. A. Guérin, A. Feix, M. Araújo, and Č. Brukner, Exponential Communication Complexity Advantage from Quantum Superposition of the Direction of Communication, Phys. Rev. Lett. **117**, 100502 (2016).
[19] A. Feix, M. Araújo, and Č. Brukner, Quantum superposition of the order of parties as a communication resource, Phys. Rev. A **92**, 052326 (2015).
[20] M. Araújo, F. Costa, and Č. Brukner, Computational Advantage from Quantum-Controlled Ordering of Gates, Phys. Rev. Lett. **113**, 250402 (2014).
[21] X. Zhao, Y. Yang, and G. Chiribella, Quantum Metrology with Indefinite Causal Order, Phys. Rev. Lett. **124**, 190503 (2020).
[22] C. Mukhopadhyay, M. K. Gupta, and A. K. Pati, Superposition of causal order as a metrological resource for quantum thermometry, arXiv:1812.07508.
[23] D. Ebler, S. Salek, and G. Chiribella, Enhanced Communication with the Assistance of Indefinite Causal Order, Phys. Rev. Lett. **120**, 120502 (2018).
[24] S. Salek, D. Ebler, and G. Chiribella, Quantum communication in a superposition of causal orders, arXiv:1809.06655.
[25] G. Chiribella, M. Banik, S. S. Bhattacharya, T. Guha, M. Alimuddin, A. Roy, S. Saha, S. Agrawal, and G. Kar, Indefinite causal order enables perfect quantum communication with zero capacity channels, New J. Phys. **23**, 033039 (2021).
[26] L. M. Procopio, A. Moqanaki, M. Araújo, F. Costa, I. A. Calafell, E. G. Dowd, D. R. Hamel, L. A. Rozema, Č. Brukner, and P. Walther, Experimental superposition of orders of quantum gates, Nat. Commun. **6**, 7913 (2015).
[27] G. Rubino, L. A. Rozema, A. Feix, M. Araújo, J. M. Zeuner, L. M. Procopio, Č. Brukner, and P. Walther, Experimental verification of an indefinite causal order, Sci. Adv. **3**, e1602589 (2017).
[28] K. Goswami, C. Giarmatzi, M. Kewming, F. Costa, C. Branciard, J. Romero, and A. G. White, Indefinite Causal Order in a Quantum Switch, Phys. Rev. Lett. **121**, 090503 (2018).
[29] Y. Guo, X.-M. Hu, Z.-B. Hou, H. Cao, J.-M. Cui, B.-H. Liu, Y.-F. Huang, C.-F. Li, G.-C. Guo, and G. Chiribella, Experimental Transmission of Quantum Information Using a Superposition of Causal Orders, Phys. Rev. Lett. **124**, 030502 (2020).
[30] K. Goswami, Y. Cao, G. A. Paz-Silva, J. Romero, and A. G. White, Increasing communication capacity via superposition of order, Phys. Rev. Research **2**, 033292 (2020).
[31] K. Wei, N. Tischler, S.-R. Zhao, Y.-H. Li, J. M. Arrazola, Y. Liu, W. Zhang, H. Li, L. You, Z. Wang, Y.-A. Chen, B. C. Sanders, Q. Zhang, G. J. Pryde, F. Xu, and J.-W. Pan, Experimental Quantum Switching for Exponentially Superior Quantum Communication Complexity, Phys. Rev. Lett. **122**, 120504 (2019).
[32] D. Felce and V. Vedral, Quantum Refrigeration with Indefinite Causal Order, Phys. Rev. Lett. **125**, 070603 (2020).
[33] M. Campisi, J. Pekola, and R. Fazio, Nonequilibrium fluctuations in quantum heat engines: Theory, example, and possible solid state experiments, New J. Phys. **17**, 035012 (2015).
[34] M. Campisi and R. Fazio, Dissipation, correlation and lags in heat engines, J. Phys. A: Math. Theor. **49**, 345002 (2016).
[35] K. Maruyama, F. Nori, and V. Vedral, Colloquium: The physics of Maxwell's demon and information, Rev. Mod. Phys. **81**, 1 (2009).

[36] C. Elouard, D. Herrera-Martí, B. Huard, and A. Auffeves, Extracting Work from Quantum Measurement in Maxwell's Demon Engines, Phys. Rev. Lett. **118**, 260603 (2017).

[37] L. Buffoni, A. Solfanelli, P. Verrucchi, A. Cuccoli, and M. Campisi, Quantum Measurement Cooling, Phys. Rev. Lett. **122**, 070603 (2019).

[38] T. Guha, M. Alimuddin, and P. Parashar, Thermodynamic advancement in the causally inseparable occurrence of thermal maps, Phys. Rev. A **102**, 032215 (2020).

[39] S. Markes and L. Hardy, Entropy for theories with indefinite causal structure, J. Phys.: Conf. Ser. **306**, 012043 (2011).

[40] K. Simonov, G. Francica, G. Guarnieri, and M. Paternostro, Work extraction from coherently activated maps via quantum switch, Phys. Rev. A **105**, 032217 (2022).

[41] G. Rubino, G. Manzano, and Č. Brukner, Quantum superposition of thermodynamic evolutions with opposing time's arrows, Commun. Phys. **4**, 251 (2021).

[42] X. Nie, X. Zhu, C. Xi, X. Long, Z. Lin, Y. Tian, C. Qiu, X. Yang, Y. Dong, J. Li *et al.*, Experimental realization of a quantum refrigerator driven by indefinite causal orders, arXiv:2011.12580.

[43] G. Chiribella, G. M. D'Ariano, P. Perinotti, and B. Valiron, Quantum computations without definite causal structure, Phys. Rev. A **88**, 022318 (2013).

[44] J.-S. Xu, M.-H. Yung, X.-Y. Xu, S. Boixo, Z.-W. Zhou, C.-F. Li, A. Aspuru-Guzik, and G.-C. Guo, Demon-like algorithmic quantum cooling and its realization with quantum optics, Nat. Photon. **8**, 113 (2014).

[45] L. Mancino, M. Sbroscia, I. Gianani, E. Roccia, and M. Barbieri, Quantum Simulation of Single-Qubit Thermometry Using Linear Optics, Phys. Rev. Lett. **118**, 130502 (2017).

[46] See Supplemental Material at http://link.aps.org/supplemental/10.1103/PhysRevResearch.4.L032029 for more experimental details, the comparison with different scenarios, as well as interpretation of our experiment by maxwell-demon-like cooling mechanism.

[47] K. A. Fisher, R. Prevedel, R. Kaltenbaek, and K. J. Resch, Optimal linear optical implementation of a single-qubit damping channel, New J. Phys. **14**, 033016 (2012).

[48] H. Lu, C. Liu, D.-S. Wang, L.-K. Chen, Z.-D. Li, X.-C. Yao, L. Li, N.-L. Liu, C.-Z. Peng, B. C. Sanders, Y.-A. Chen, and J.-W. Pan, Experimental quantum channel simulation, Phys. Rev. A **95**, 042310 (2017).

[49] A. B. Pippard, *Elements of Classical Thermodynamics: For Advanced Students of Physics* (Cambridge University Press, Cambridge, 1964).

[50] K. Abdelkhalek, Y. Nakata, and D. Reeb, Fundamental energy cost for quantum measurement, arXiv:1609.06981.

[51] R. Landauer, Irreversibility and heat generation in the computing process, IBM J. Res. Dev. **5**, 183 (1961).

[52] M. Perarnau-Llobet, K. V. Hovhannisyan, M. Huber, P. Skrzypczyk, N. Brunner, and A. Acín, Extractable Work from Correlations, Phys. Rev. X **5**, 041011 (2015).

[53] G. Francica, J. Goold, F. Plastina, and M. Paternostro, Daemonic ergotropy: Enhanced work extraction from quantum correlations, npj Quantum Inf. **3**, 12 (2017).

[54] E. Chitambar and G. Gour, Quantum resource theories, Rev. Mod. Phys. **91**, 025001 (2019).

[55] J. Bavaresco, M. Araújo, Č. Brukner, and M. T. Quintino, Semi-device-independent certification of indefinite causal order, Quantum **3**, 176 (2019).

[56] B. Swingle, G. Bentsen, M. Schleier-Smith, and P. Hayden, Measuring the scrambling of quantum information, Phys. Rev. A **94**, 040302(R) (2016).

[57] G. Zhu, M. Hafezi, and T. Grover, Measurement of many-body chaos using a quantum clock, Phys. Rev. A **94**, 062329 (2016).